ChemComm

COMMUNICATION

View Article Online
View Journal | View Issue

Cite this: *Chem. Commun.*, 2016, 52, 4718

Received 18th November 2015,
Accepted 25th February 2016

DOI: 10.1039/c5cc09552b

www.rsc.org/chemcomm

A fluorescent surrogate of thymidine in duplex DNA†

Guillaume Mata, Olivia P. Schmidt and Nathan W. Luedtke*

^{DMA}T is a new fluorescent thymidine mimic composed of 2′-deoxyuridine fused to dimethylaniline. ^{DMA}T exhibits the same pK_a and base pairing characteristics as native thymidine residues, and its fluorescence properties are highly sensitive to nucleobase ionization, base pairing and metal binding.

Nucleobase analogs constitute an important family of fluorescent probes.[1] They can be positioned in nucleic acid structures with high precision, and their photophysical properties are highly sensitive to local polarity,[2] viscosity,[3] and pH.[4] These features facilitate specific monitoring of biochemical transformations,[5] conformational changes,[6] metal binding,[7] and base pairing interactions.[8]

Nucleobase ionization can mediate proton-coupled folding,[9] metal binding,[10] and/or the catalytic activities of certain nucleic acids at neutral pH.[11] Thymidine (T) and uracil (U) are among the most inherently acidic residues,[12] but fluorescent analogs capable of reporting pyrimidine ionization in nucleic acids are scarce. Previously reported examples utilized biaryl or triaryl fluorophores,[4c,d] having unreported or highly perturbed pK_a values (pK_a ≈ 6.8) as compared to unmodified T and U residues (pK_a ≈ 9.5).[12] Here we report "*N*,*N*-dimethylaniline-2′-deoxythymidine" or "^{DMA}T" that exhibits the same pK_a and base pairing characteristics as thymidine, as well as fluorescence properties that can be used to monitor nucleobase ionization, base pairing and metal binding reactions in DNA.

^{DMA}T was designed to have the same Watson–Crick face and pK_a as thymidine. To generate a push–pull fluorophore, an electron donating group was incorporated at the C6 position of a quinazoline core.[9,13] This position was selected because it is not in conjugation with N3–H, and therefore expected to have little or no impact on its acidity. Molecular orbital calculations predicted charge transfer from a dimethylaniline-centered HOMO to a pyrimidine-centered LUMO with a HOMO–LUMO energy gap (ΔE) = 2.44 eV (Fig. 1). ^{DMA}T was therefore predicted to be a "push–pull" fluorophore in its neutral form. In contrast, the ^{DMA}T anion has a pyrimidine-centered HOMO, and a larger ΔE = 2.81 eV. We therefore expected a blue-shift in ^{DMA}T fluorescence upon its deprotonation.

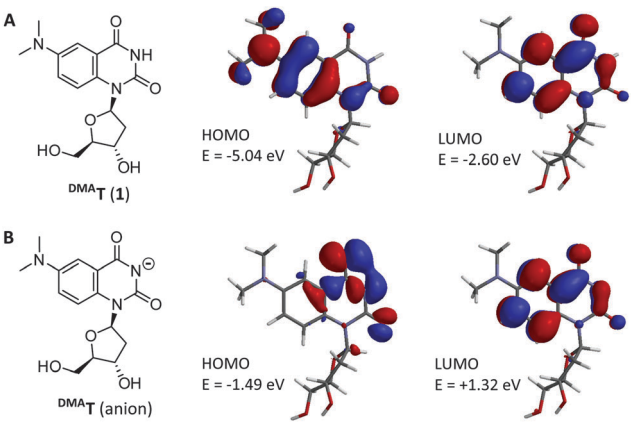

Fig. 1 Structure of the ^{DMA}T nucleoside (A), and its conjugate base (B). HOMOs, LUMOs, and their relative energies were calculated from DFT-optimized geometries using LSDA/pBP86/DN**.

The synthesis of ^{DMA}T (**1**) commenced from the previously-reported nucleoside **2** (Scheme 1).[14] Buchwald–Hartwig coupling with Me_2NH gave the known compound **3** in 82% yield.[9] Addition of fluoride ions to **3** afforded the new nucleoside ^{DMA}T (**1**) in a

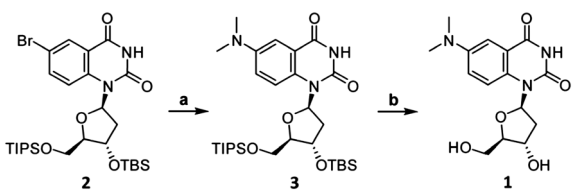

Scheme 1 Synthesis of ^{DMA}T (**1**). Reaction conditions: (a) Me_2NH, $Pd_2(dba)_3$ (5 mol%), JohnPhos (20 mol%), KOtBu, THF, dioxane, 60 °C, 2 h, 82% yield. (b) TBAF, THF, 23 °C, 2 h, 62% yield.

Department of Chemistry, University of Zurich, Winterthurerstrasse 190, CH-8057 Zurich, Switzerland. E-mail: nathan.luedtke@chem.uzh.ch

† Electronic supplementary information (ESI) available. See DOI: 10.1039/c5cc09552b

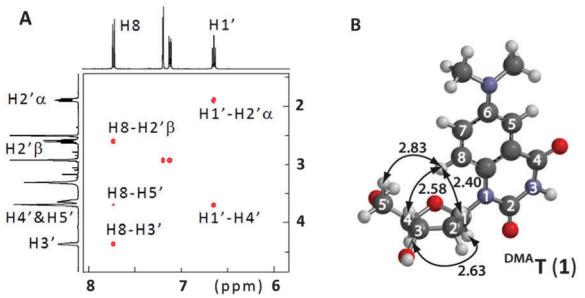

Fig. 2 (A) Partial ^{1}H–^{1}H 2D ROESY of ^{DMA}T (**1**) in DMSO-d_6. See ESI† for complete spectrum. (B) Energy-minimized conformation of ^{DMA}T according to DFT calculations (B3LYP/6-311G*). ^{1}H–^{1}H distances are shown in Å.

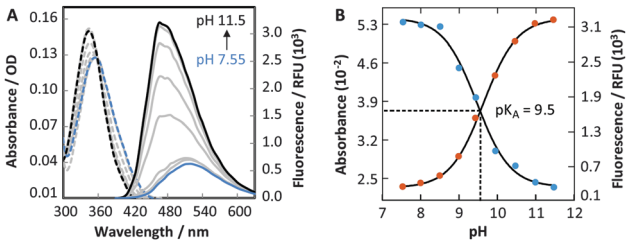

Fig. 3 (A) Absorbance (- - -) and emission (—) spectra (λ_{ex} = 360 nm) of 40 μM ^{DMA}T (**1**) in phosphate citric acid buffer (200 mM of Na_2HPO_4, 100 mM of citric acid and 100 mM NaCl). (B) Single-wavelength analyses of the pH-dependent absorbance (400 nm, blue dots) and emission (470 nm, red dots) of ^{DMA}T (**1**).

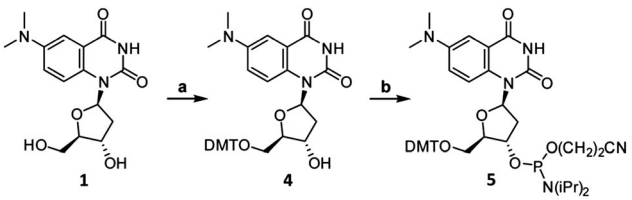

Scheme 2 Synthesis of ^{DMA}T phosphoramidite (**5**). Reaction conditions: (a) DMT-Cl, pyridine, 23 °C, 45 min, 79% yield. (b) 2-Cyanoethyl-*N*,*N*-diisopropyl-chlorophosphoramidite, DIPEA, CH_2Cl_2, 0 °C to 23 °C, 45 min, 86% yield. See ESI† for synthetic details and characterizations.

62% yield (see ESI† for synthetic details and characterization). ^{1}H–^{1}H ROESY cross-peaks were observed between H8–H5′, H8–H3′, and H8–H2′β of ^{DMA}T (**1**), indicating an *anti*-conformation of the nucleobase (Fig. 2). Cross-peaks were also observed between H1′–H4′, which confirmed the β-stereochemistry of the anomeric position.[14] ^{DMA}T (**1**) therefore possesses the same glycosidic bond conformation and stereochemistry as 2′-deoxythymidine.

Under neutral conditions, ^{DMA}T (**1**) exhibits an exceptionally large Stoke's shift, with an absorbance maximum (λ_{abs}) = 357 nm and emission maximum (λ_{em}) = 522 nm (Table 1). To characterize its environmental sensitivity, the λ_{abs} and λ_{em} of ^{DMA}T (**1**) were measured in various water/dioxane mixtures (Table S2 and Fig. S1, ESI†). A linear correlation (R^2 = 0.980) with a large slope of 177 cm^{-1} kcal^{-1} mol^{-1} was obtained by plotting the Stoke's shift of ^{DMA}T (**1**) against Reichardt's solvent polarity parameter (E_T^{30}).[15,16] Together these results confirm that ^{DMA}T (**1**) is a push–pull fluorophore. Interestingly, ^{DMA}T (**1**) exhibits a two-fold higher quantum yield in D_2O (ϕ = 0.07) than H_2O (ϕ = 0.03, Table 1), suggesting that proton transfer with bulk solvent provides an effective nonradiative decay pathway.[7a]

To evaluate the fluorescence sensitivity of ^{DMA}T (**1**) towards nucleobase ionization, its absorbance and emission spectra were recorded at different pH values. Consistent with DFT calculations, the emission maximum of ^{DMA}T (**1**) shifted towards the blue with increasing pH (Fig. 3A). This was accompanied by a dramatic increase in fluorescence intensity. The absorbance and fluorescence changes were plotted against pH to determine a pK_a = 9.5 ± 0.1, Fig. 3B. This value corresponds to the pK_a of thymidine and uracil.[12]

To facilitate the site-specific incorporation of ^{DMA}T into DNA, phosphoramidite **5** was prepared in two steps by standard DMT-protection and phosphitylation reactions (Scheme 2). Using automated DNA synthesis, ^{DMA}T was incorporated at one of four positions within the same, 21-residue DNA sequence (Table S3, ESI†). Three positions near the middle of the sequence (**X13**, **X14** and **X15**) and a single position near the 5′ terminus (**X2**) were selected in order to evaluate the impacts of variable flanking sequences and DNA end "breathing" motions, respectively.‡ The identity and purity of the purified oligonucleotides were confirmed using analytical HPLC and HR-MS (Table S4 and Fig. S2, ESI†).

Table 1 Photophysical data of ^{DMA}T (**1**) and its conjugate base

Solvent	λ_{abs} [a]	λ_{em} [b]	$\varepsilon_{(260)}$ [c]	$\varepsilon_{(\lambda_{abs})}$ [c]	ϕ [d]
H_2O	357	522	15.0	2.9	0.03
pH = 11.0	345	480	17.1	3.9	0.09
D_2O	355	520	13.0	2.7	0.07
pD = 11.0	345	480	14.3	3.4	0.19

[a] Absorbance maxima (λ_{abs}) in nm. [b] Emission maxima (λ_{em}) in nm. [c] Extinction coefficients (ε) in 10^3 M^{-1} cm^{-1} were measured at 260 nm and at λ_{abs}. [d] Quantum yields (ϕ) were calculated using quinine hemisulfate in 0.5 M H_2SO_4 as a fluorescent standard.[17] Reproducibility is within ±10% of each reported ϕ value.

Circular dichroism (CD) and thermal denaturation experiments were used to assess the impact of ^{DMA}T on the global structure and stability of duplex DNA. ^{DMA}T-containing duplexes were prepared by heating and slow cooling with 1.1 equiv. of the complementary strand to give CD spectra consistent with the formation of B-form helices (Fig. S3, ESI†).[18] CD spectra were monitored as a function of temperature (Fig. S4, ESI†) to determine the melting temperature of each duplex (T_m, Table 2). ^{DMA}T–A-containing duplexes exhibited nearly identical T_m values as the corresponding wild-type duplexes containing T–A base pairs (ΔT_m = −0.2 to −1.7 °C). In contrast, duplexes containing a single C–A, A–A, ^{DMA}T–T or T–T mismatch at positions **X13**–**X15** caused a large loss in thermal stability (ΔT_m = −4.8 to −7.9 °C). End breathing motions of duplex DNA explain the relatively small changes when the mismatches were positioned at **X2** (Table 2).

The fluorescence properties of ^{DMA}T were highly sensitive to the global structure of the DNA containing it (Fig. S5, ESI,† and Table 3). At all three internal positions **X13**–**X15**, ^{DMA}T exhibited a two-fold higher quantum yield and blue-shifted λ_{em} in duplex

Table 2 Thermal denaturation melting (T_m) temperatures (°C) of duplexes[a]

Position	T–A	^{DMA}T–A	C–A	A–A	^{DMA}T–T	T–T
X2	69.0	68.8	67.3	67.5	68.0	67.0
X13	68.8	67.1	60.9	62.4	62.3	61.5
X14	68.7	67.3	61.3	63.9	62.5	61.5
X15	68.9	68.0	61.2	62.7	64.0	62.8

[a] All samples contained 5 μM of DNA in phosphate citric acid buffer (200 mM of Na_2HPO_4, 100 mM of citric acid, and 100 mM NaCl or $NaNO_3$) at pH = 7.35. Reproducibility is within ±0.3 °C of each reported value. See Table S3, ESI for duplex sequences.

versus single-stranded DNA. Decreased probe hydration upon duplex formation is probably responsible for these differences, because the ^{DMA}**T** nucleoside (**1**) exhibited higher quantum yields and blue-shifted λ_{em} in organic *versus* aqueous solvents (Table S2 and Fig. S1, ESI†). At all four positions of incorporation, higher fluorescence anisotropy was observed in duplex DNA (r = 0.09–0.18) as compared to unfolded structures (r = 0.03–0.06), consistent with large losses in dynamic motions of the probe upon duplex formation (Table 3).

The photophysical properties of ^{DMA}**T** were sensitive to matched *versus* mismatched base pairing in duplex DNA. ^{DMA}**T** exhibited a higher quantum yield and blue-shifted λ_{abs} and λ_{em} in ^{DMA}**T**–A base pairs as compared to ^{DMA}**T**–T, ^{DMA}**T**–G and ^{DMA}**T**–C mismatches (Table 4). Changes in probe hydration and base stacking are likely responsible for these differences, because similar trends were also observed when comparing duplex *versus* single-stranded DNA containing ^{DMA}**T** (Table 3). Taken together with the thermal denaturation results (Table 2), these data provide additional evidence that ^{DMA}**T** exhibits the same base pairing specificity as T.

Metal-mediated base pairing interactions serve as important recognition motifs in biological and material sciences.[10] For example, Hg^{II} ions specifically bind to opposing thymine residues to form T–Hg–T base pairs[19] that can cause miscoding of DNA synthesis *in vitro* and possibly *in vivo*.[20] To evaluate the ability of ^{DMA}**T**–T to mimic T–T in duplex DNA, T_m values were measured in the presence or absence of 1.0 equiv. of Hg^{II} (Table 5 and Fig. S6–S8, ESI†). Only small increases in thermal stabilities (ΔT_m = +0.8 to +1.5 °C) were observed when Hg^{II} was added to duplexes containing a ^{DMA}**T**–T or T–T at position **X2**, whereas much larger increases were observed at positions **X13–X15** (ΔT_m = +2.9 to +6.0 °C). At all four positions, the same T_m values were obtained for duplexes containing ^{DMA}**T**–Hg–T as T–Hg–T. In contrast, the addition of 1.0 equiv. of Hg^{II} to duplexes containing a C–T mismatch resulted in no increase in thermal stability as compared to the mismatch alone (Table 5). Taken together, these results demonstrate the excellent mimicry of ^{DMA}**T** for thymidine residues in the demanding context of T–Hg^{II}–T base pairs.

Table 3 Photophysical properties of ^{DMA}**T** in DNA (**X** = ^{DMA}**T**)

Structure	Position	λ_{abs}[a]	λ_{em}[b]	r[c]	ϕ[d]
Duplex	**X2**	355	505	0.18	0.03
	X13	355	504	0.09	0.20
	X14	355	492	0.14	0.13
	X15	355	486	0.15	0.11
Unfolded	**X2**	365	515	0.03	0.05
	X13	365	515	0.05	0.09
	X14	365	516	0.06	0.06
	X15	365	515	0.05	0.05

[a] Absorbance maxima (λ_{abs}) in nm. [b] Emission maxima (λ_{em}) in nm. [c] Fluorescence anisotropy (r) with λ_{ex} = 375 nm and λ_{em} = 500 nm. [d] Quantum yields (ϕ) calculated using the ^{DMA}**T** nucleoside (ϕ = 0.03) as a fluorescent standard. Reproducibility is within ±30% of each reported ϕ value. All samples contained 4 μM of DNA in a buffer containing 20 mM of Na_2HPO_4, 10 mM of citric acid and 10 mM NaCl (pH = 7.35). See Table S3, ESI for duplex sequences.

Table 4 Photophysical properties of ^{DMA}**T** in duplex DNA[a]

Position	Pairing	λ_{abs}	λ_{em}	r	ϕ
X13	^{DMA}**T**–A	355	504	0.09	0.20
	^{DMA}**T**–T	365	505	0.09	0.13
	^{DMA}**T**–G	365	508	0.10	0.09
	^{DMA}**T**–C	365	498	0.10	0.12
X15	^{DMA}**T**–A	355	486	0.15	0.11
	^{DMA}**T**–T	365	500	0.12	0.08
	^{DMA}**T**–G	370	505	0.12	0.06
	^{DMA}**T**–C	370	502	0.17	0.05

[a] See Table 3 footnotes for experimental details and symbol definitions.

Table 5 Thermal denaturation melting (T_m) temperatures (°C) of duplexes[a]

Position	T–T	T–T + Hg^{II}	^{DMA}T–T	^{DMA}T–T + Hg^{II}	C–T	C–T + Hg^{II}
X2	67.0	68.5	68.0	68.8	66.8	66.3
X13	61.5	67.5	62.3	67.1	60.4	61.1
X14	61.5	65.1	62.5	65.7	60.4	60.3
X15	62.8	65.7	64.0	66.9	60.6	60.9

[a] See Table 2 footnotes for experimental details.

The fluorescence properties of ^{DMA}**T** can be utilized to monitor site-specific binding of Hg^{II} ions to ^{DMA}**T**–T sites. Bi-phasic fluorescence quenching was observed upon addition of Hg^{II} to duplex DNA containing a ^{DMA}**T**–T mismatch, giving a 95% decrease in fluorescence intensity upon addition of 3 equiv. of Hg^{II} (Fig. 4). Similar results were obtained when ^{DMA}**T** was located at all four positions **X2**, **X13**, **X14** and **X15** (Table S5 and Fig. S9, ESI†). The biphasic quenching (Fig. 4B) mirrors the increases in T_m values obtained when Hg^{II} is added to duplexes containing a T–T mismatch (Fig. S6, ESI†). A comparison of these results reveals that the steep slopes observed between 0.0 to 1.0 equiv. of added Hg^{II} are a result of T–T-specific binding, and the shallow slopes

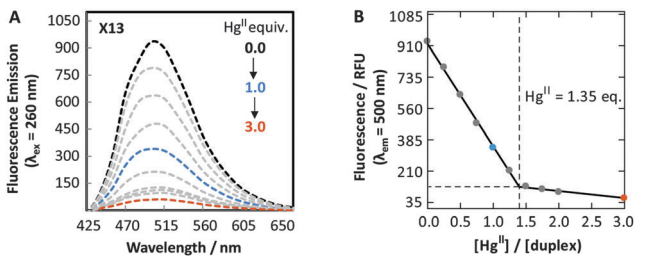

Fig. 4 (A) Fluorescence spectra (λ_{ex} = 260 nm) of duplex **X13** in the absence (black) and in the presence of variable $Hg(ClO_4)_2$. (B) Plot of fluorescence intensity (λ_{em} = 500 nm) *versus* equiv. of Hg^{II} ions. All samples contained 5 μM of DNA in phosphate citric acid buffer (200 mM of Na_2HPO_4, 100 mM of citric acid and 100 mM $NaNO_3$) at pH = 7.35. See Table S3, ESI† for duplex sequences.

between 2.0 to 3.0 equiv. are due to non-specific interactions. In contrast to ^{DMA}**T**–T, very little fluorescence quenching (−20%) was observed upon the addition of Hg^{II} ions to duplex DNA containing a ^{DMA}**T**–A base pair, or a ^{DMA}**T**–G mismatch (Table S6 and Fig. S10, ESI†). Conversely, the addition of Zn^{II}, Cu^{II}, Mg^{II}, Fe^{II}, Ca^{II}, Ag^{I}, Cd^{II}, Pd^{II} and Ni^{II} ions to duplexes containing a ^{DMA}**T**–T mismatch resulted in little or no change in ^{DMA}**T** fluorescence (Fig. S11, ESI†). These results are consistent with previous studies demonstrating a high degree of specificity between T–T mismatches and Hg^{II} ions using thermal denaturation.[19] To the best of our knowledge, our results provide the first example of using a fluorescent nucleobase analog to monitor a specific binding reaction between DNA and Hg^{II} ions. ^{DMA}**T** will therefore enable detailed kinetics analyses and large-scale screening efforts that are not feasible using other analytical techniques.[10d]

A variety of fluorescent nucleoside analogs are available for solid-phase synthesis of DNA and RNA.[1–8] However, the vast majority of these probes are quenched by their incorporation into duplex nucleic acids, where they can disrupt duplex stability by as much as a base pair mismatch. Here we report a new fluorescent thymidine mimic composed of 2′-deoxyuridine fused to dimethylaniline. According to thermal denaturation, fluorescence, and metal binding studies, ^{DMA}**T** exhibits the same base pairing characteristics as native thymidine residues. The quantum yield of ^{DMA}**T** (ϕ = 0.03 in water) increases upon its incorporation into duplex DNA (ϕ = 0.11–0.20), where its fluorescence properties are highly sensitive to nucleobase hydration, ionization, base pairing, and metal binding. Taken together, these results demonstrate that ^{DMA}**T** will enable a wide variety of studies aimed at characterizing biochemical transformations, conformational changes, site-specific metal binding, and base pairing interactions with single-nucleotide resolution.

Notes and references

‡ DNA sequences: **X2**: C**X**C-TAA-CCC-TAA-CCC-TAA-CCC; **X13**: CCC-TAA-CCC-TAA-**X**CC-TAA-CCC; **X14**: CCC-TAA-CCC-TAA-**CX**C-TAA-CCC; **X15**: CCC-TAA-CCC-TAA-CC**X**-TAA-CCC; (**X** = ^{DMA}**T**, T (wt), C or A).

1 (*a*) M. E. Hawkins, *Cell Biochem. Biophys.*, 2001, **34**, 257; (*b*) A. T. Krueger, H. Lu, A. H. Lee and E. T. Kool, *Acc. Chem. Res.*, 2007, **40**, 141; (*c*) R. W. Sinkeldam, N. J. Greco and Y. Tor, *Chem. Rev.*, 2010, **110**, 2579; (*d*) L. M. Wilhelmsson, *Q. Rev. Biophys.*, 2010, **43**, 159; (*e*) A. A. Tanpure, M. G. Pawar and S. G. Srivatsan, *Isr. J. Chem.*, 2013, **53**, 366; (*f*) M. Weinberger, F. Berndt, R. Mahrwald, N. P. Ernsting and H. A. Wagenknecht, *J. Org. Chem.*, 2013, **78**, 2589; (*g*) A. Matarazzo and R. H. E. Hudson, *Tetrahedron*, 2015, **71**, 1627.
2 R. W. Sinkeldam, N. J. Greco and Y. Tor, *ChemBioChem*, 2008, **9**, 706.
3 R. W. Sinkeldam, A. J. Wheat, H. Boyaci and Y. Tor, *ChemPhysChem*, 2011, **12**, 567.
4 (*a*) K. M. Sun, C. K. McLaughlin, D. R. Lantero and R. A. Manderville, *J. Am. Chem. Soc.*, 2007, **129**, 1894; (*b*) D. Jiang and F. Seela, *J. Am. Chem. Soc.*, 2010, **132**, 4016; (*c*) J. Riedl, R. Pohl, L. Rulisek and M. Hocek, *J. Org. Chem.*, 2012, **77**, 1026; (*d*) R. W. Sinkeldam, P. A. Hopkins and Y. Tor, *ChemPhysChem*, 2012, **13**, 3350.
5 (*a*) R. A. Mizrahi, D. Shin, R. W. Sinkeldam, K. J. Phelp, A. Fin, D. J. Tantillo, Y. Tor and P. A. Beal, *Angew. Chem., Int. Ed.*, 2015, **54**, 8713; (*b*) A. C. Jones and R. K. Neely, *Q. Rev. Biophys.*, 2015, **48**, 244.
6 (*a*) F. Godde, J. J. Toulmé and S. Moreau, *Biochemistry*, 1998, **37**, 13765; (*b*) Y. Hikida, M. Kimoto, S. Yokoyama and I. Hirao, *Nat. Protoc.*, 2010, **5**, 1312; (*c*) A. Dumas and N. W. Luedtke, *Nucleic Acids Res.*, 2011, **39**, 6825; (*d*) A. Dumas and N. W. Luedtke, *ChemBioChem*, 2011, **12**, 2044; (*e*) M. Sholokh, R. Sharma, D. Shin, R. Das, O. A. Zaporozhets, Y. Tor and Y. Mély, *J. Am. Chem. Soc.*, 2015, **137**, 3185; (*f*) A. A. Tanpure and S. G. Srivatsan, *Nucleic Acids Res.*, 2015, **43**, e149.
7 (*a*) A. Dumas and N. W. Luedtke, *Chem. – Eur. J.*, 2012, **18**, 245; (*b*) A. Omumi, C. K. McLaughlin, D. Ben-Israel and R. A. Manderville, *J. Phys. Chem. B*, 2012, **116**, 6158; (*c*) S. K. Jana, X. Guo, H. Mei and F. Seela, *Chem. Commun.*, 2015, **51**, 17301.
8 (*a*) J. Michel, G. Gueguen, J. Vercauteren and S. Moreau, *Tetrahedron*, 1997, **53**, 8457; (*b*) A. Okamoto, K. Tainaka and I. Saito, *J. Am. Chem. Soc.*, 2003, **125**, 4972; (*c*) H.-A. Wagenknecht, *Ann. N. Y. Acad. Sci.*, 2008, **1130**, 122; (*d*) Y. Xie, A. V. Dix and Y. Tor, *J. Am. Chem. Soc.*, 2009, **131**, 17605; (*e*) N. J. Greco, R. W. Sinkeldam and Y. Tor, *Org. Lett.*, 2009, **11**, 1115; (*f*) X. Ming and F. Seela, *Chem. – Eur. J.*, 2012, **18**, 9590; (*g*) Y. Saito, A. Suzuki, Y. Okada, Y. Yamasaka, N. Nemoto and I. Saito, *Chem. Commun.*, 2013, **49**, 5684.
9 G. Mata and N. W. Luedtke, *J. Am. Chem. Soc.*, 2015, **137**, 699.
10 (*a*) G. H. Clever, C. Kaul and T. Carell, *Angew. Chem., Int. Ed.*, 2007, **46**, 6226; (*b*) J. Müller, *Metallomics*, 2010, **2**, 318–327; (*c*) G. H. Clever and M. Shionoya, *Met. Ions Life Sci.*, 2012, **10**, 269; (*d*) Y. Tanaka, J. Kondo, V. Sychrovský, J. Šebera, T. Dairaku, H. Saneyoshi, H. Urata, H. Torigoe and A. Ono, *Chem. Commun.*, 2015, **51**, 17343.
11 (*a*) P. L. Nixon and D. P. Giedroc, *J. Mol. Biol.*, 2000, **296**, 659; (*b*) S. R. Das and J. A. Piccirilli, *Nat. Chem. Biol.*, 2005, **1**, 45.
12 R. M. Izatt, J. J. Christensen and H. Rytting, *Chem. Rev.*, 1971, **71**, 439.
13 (*a*) Y. Xie, T. Maxson and Y. Tor, *J. Am. Chem. Soc.*, 2010, **132**, 11896; (*b*) G. Mata and N. W. Luedtke, *Org. Lett.*, 2013, **15**, 2462; (*c*) D. Liu, Z. Y. Zhang, H. Z. Zhang and Y. Wang, *Chem. Commun.*, 2013, **49**, 10001; (*d*) S. Achelle, J. Rodriguez-Lopez and F. Robin-le Guen, *J. Org. Chem.*, 2014, **79**, 7564.
14 G. Mata and N. W. Luedtke, *J. Org. Chem.*, 2012, **77**, 9006.
15 (*a*) C. Reichardt, *Chem. Rev.*, 1994, **94**, 2319; (*b*) R. W. Sinkeldam and Y. Tor, *Org. Biomol. Chem.*, 2007, **5**, 2523.
16 (*a*) T. L. Netzel, M. Zhao, K. Nafisi, J. Headrick, M. S. Sigman and B. E. Eaton, *J. Am. Chem. Soc.*, 1995, **117**, 9119; (*b*) R. S. Butler, P. Cohn, P. Tenzel, K. A. Abboud and R. K. Castellano, *J. Am. Chem. Soc.*, 2009, **131**, 623.
17 W. H. Melhuish, *J. Phys. Chem.*, 1961, **65**, 229.
18 (*a*) D. M. Gray, R. L. Ratliff and M. R. Vaughan, *Methods Enzymol.*, 1992, **211**, 389; (*b*) J. Kypr, I. Kejnovska, D. Renciuk and M. Vorlickova, *Nucleic Acids Res.*, 2009, **37**, 1713.
19 Y. Miyake, H. Togashi, M. Tashiro, H. Yamaguchi, S. Oda, M. Kudo, Y. Tanaka, Y. Kondo, R. Sawa, T. Fujimoto, T. Machinami and A. Ono, *J. Am. Chem. Soc.*, 2006, **128**, 2172.
20 H. Urata, E. Yamaguchi, T. Funai, Y. Matsumura and S. Wada, *Angew. Chem., Int. Ed.*, 2010, **49**, 6516.